Nanoscale

Accepted Manuscript

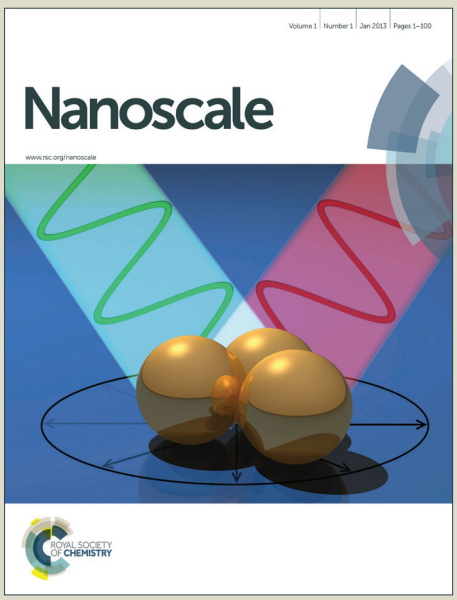

ROYAL SOCIETY OF CHEMISTRY

www.rsc.org/nanoscale

Kinetically Controlled Synthesis of Large-Scale Morphology-Tailored Silver Nanostructures at Low Temperature

Ling Zhang,[a,b,†] Yuda Zhao,[a] Ziyuan Lin,[a] Fangyuan Gu,[a] Shu Ping Lau,[a] Li Li,*[,b] and Yang Chai*[,a,c]

[a]Department of Applied Physics, The Hong Kong Polytechnic University, Hung Hom, Kowloon, Hong Kong, China
[b]Institute of Textiles & Clothing, The Hong Kong Polytechnic University, Hung Hom, Kowloon, Hong Kong, China
[c]The Hong Kong Polytechnic University Shenzhen Research Institute Shenzhen, China

ABSTRACT: Ag nanostructures are widely used in catalysis, energy conversion and chemical sensing. Morphology-tailored synthesis of Ag nanostructures is critical to tune the physical and chemical properties. In this study, we develop a method for synthesizing the morphology-tailored Ag nanostructures in aqueous solution at a low temperature (45°C). With the use of AgCl nanoparticles as the precursors, the growth kinetics of Ag nanostructures can be tuned with the pH value of solution and the concentration of Pd cubes which catalyze the reaction. Ascorbic acid and cetylpyridium chloride are used as the mild reducing agent and capping agent in aqueous solution, respectively. High-yield Ag nanocubes, nanowires, right triangular bipyramids/cubes with twinned boundaries, and decahedra are successfully produced, respectively. Our method opens up a new environmentally-friendly and economical route to synthesize large-scale and morphology-tailored Ag nanostructures, which is significant to the controllable fabrication of Ag nanostructures and fundamental understanding of the growth kinetics.

INTRODUCTION

Silver (Ag) nanostructures play important roles in catalysis, electronics, photonics, energy conversion and chemical sensing owing to their unique electronic and optical properties.[1-6] The properties of Ag nanostructures heavily depends on their physical parameters, including size, shape, composition, and structure. For example, Ag nanostructures exhibit surface plasmon resonances and lead to significant enhancement of Raman scatting, fluorescence emitting, and circular dichroism absorption of biomolecules.[7-11] The resonance peak and enhancement factor are closely related to the morphology of the Ag nanostructures.[12-14] In addition, Ag nanowire networks have been regarded as a promising transparent conductor alternative to the hard indium tin oxide because of their good conductivity, transmittance, and flexibility.[15,16] Bergin et al. have shown that the dimensions of Ag nanowires affect both transmittance and sheet resistance of a random nanowire network.[17,18] Therefore, it is essential to develop methods to precisely control the morphology of Ag nanostructures for practical applications. Bottom-up colloidal methods are favorable in large-scale and low-cost synthesis of metal nanostructures with controllable morphology.[19-21] Currently, polyol synthesis methods are the most common routes to fabricate large-scale colloidal Ag nanostructures, such as, nanowires, nanocubes, triangular bipyramids, octahedra, or plates.[22-24] In the methods, polyol solvents, e.g. ethylene glycol, is preheated to the boiling point (>140 °C) and is oxidized into aldehyde as the reducing agent. Ag nanostructures are generated by reducing silver precursor (e.g., silver nitrate) in the presence of poly(vinyl pryrrolidone) capping agents.[25-27] The morphology of Ag nanostructures is not easily controlled in aqueous solution because the explosive formation of Ag atoms is quickly aggregated into large particles. The growth processes of metal nanostructures are affected by both thermodynamic (e.g., temperature, surface energy) and kinetic (e.g., reaction rate, concentration) factors in aqueous solution.[28] For example, with the nanocrystalline particles as the precursor, the nucleation rate of metal atoms are retarded moderately, which facilitate the controllable morphology deviated from those favored by thermodynamics.[29,30]

In this work, we use crystalline silver chloride (AgCl) nanoparticles as the precursors and cetylpyridinium chloride (CPC) as the capping agent to synthesize large-scale Ag nanostructures at a low temperature (45 °C). Ascorbic acid (Asa) is a mild, high-efficiency, and water-soluble reducing agent, which can be injected in the CPC solution and enables the formations of Ag nanostructures at a low temperature. By adjusting the pH value of the solution, and the concentration of the palladium (Pd) nanocubes, we successfully synthesize Ag nanostructures with various shapes, including nanocubes, nanowires, right-triangular

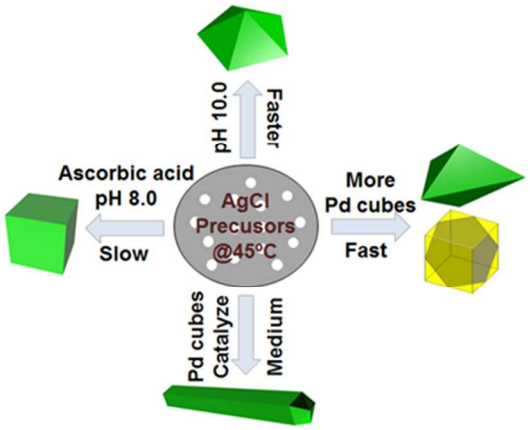

Scheme 1. Morphology-controlled synthesis of Ag nanostructures.

bipyramid, and decahedra, as shown in Scheme 1. {100} Ag facet is the thermodynamically stable facet in CPC solution, and the reaction rate determines the anisotropic characteristics of Ag nanostructures at the pH value of 8.0. Ag nanoclusters are formed directly by the reduction of Asa and slowly aggregate into {100}-faceted Ag nanocubes. Pd nanocubes can catalyze the reduction process and promote the formations of one-dimensional Ag nanowires. Five-fold twinned Ag nanowires (the aspect ratio of 136) with {100} side facets are produced with less Pd nanocubes. And thermodynamically favored polyhedral Ag nanostrucrues, {100}-faceted right-bipyramids and nanocubes (35.3 nm) with twinned boundaries are produced with more Pd nanocubes. By increasing the pH value of the solution to 10.0, the reduction process become faster and the kinetically controlled {111}-faceted decahedral Ag nanoparticles are produced. Compared to the polyol synthesis routes, this method possess the following advantages, (1) Water is used as the solvent, and the organic solvents (e.g. ethylene glycol) are not necessary; (2) the temperature is as low as 45 °C, to which Polyol synthesis routes never reach; (3) the products are water-soluble and acetone is not used in the post-treatment. Our method opens up a new environmentally-friendly route to synthesize large-scale and morphology-tailored Ag nanostructures in a much broader range by a convenient yet reproducible method.

EXPERIMETAL SECTION

Chemicals and Solutions. Palladium(II) chloride ($PdCl_2$), silver nitrate ($AgNO_3$), ascorbic acid (Asa), cetyltrimethylammonium bromide (CTAB), cetylpyridinium chloride (CPC), and potassium bromide (KBr) were purchased from Sinopharm Chemical Reagent Co. Ltd. (Shanghai, China). Hydrochloride acid (HCl, 37%) was purchased from RLCF Limited. Ammonium hydroxide solution (NH_4OH, 25% NH_3 basis) was purchased from American Regent. All the chemicals were of analytical grade. Double-deionized water (18.2 MΩ cm) was used to prepare all aqueous solutions. A 10 mM H_2PdCl_4 solution was prepared by dissolving 0.0355 g $PdCl_2$ in 2 mL of 0.2 M HCl solution and further diluting into 20 mL with double-deionized water.

Instruments. SEM images were taken using a JEOL JSM-633F at 5 kV. TEM images, HRTEM microscopy image, SAED pattern, high-angle annular dark-field scanning TEM images, and elemental mapping images were taken using a JEOL Model JEM-2100F microscope operated at 200 kV. XRD data were collected using Rigaku SmartLab (Cu Kα radiation). UV-vis extinction and transmittance spectra were obtained using Shimadzu UV-2550 Spectrophotometers.

Synthesis of Pd nanocubes. Pd nanocubes with the diameter around 22 nm were synthesized using the method reported previously.[31] Briefly, a 500 μL aliquot of 10 mM H_2PdCl_4 solution was added to 9.42 mL of 12.5 mM CTAB aqueous solution, which was heated at 95 °C under stirring. After 5 min, 80 μL freshly prepared 100 mM Asa aqueous solution was added, and the reaction continued for 20 min. The Pd nanocubes with the side length of 22 nm were washed for one time with 5 mM CPC aqueous solution and kept at 27 °C for future use. The concentration of Pd nanocubes was 66.4 nM. And the TEM image of Pd nanocubes produced are shown in Figure S1.

Synthesis of Ag nanostructures. AgCl nanoparticles and CPC were used as the precursors and the capping agents, respectively, to synthesize Ag nanostructures with different shapes. First, 5 mL CPC solution (5 mM) was mixed with 300 μL aliquot of the $AgNO_3$ solution (10 mM) at 40 °C, and then white suspension of AgCl was formed gradually. After 25-min reaction, 600 μL aliquot of Asa solution (100 mM) was added. The solution was mix thoroughly and the reaction proceeded for 11 hours. Yellow suspension of the Ag nanocubes with 204 nm was obtained finally. In the synthesis of Ag nanowires, 2.5 μL aliquot of cubic Pd nanoparticles solution was introduced before Asa was added, the other procedures are the same as those in the synthesis of Ag nanocubes with 204 nm. The reaction proceeded for 4.5 hours, and milk yellow suspension was formed finally. In the synthesis of Ag right-triangular bipyramids and cubes with twinned boundaries, 100 μL aliquot of cubic Pd nanoparticles solution was introduced before Asa was added, the other procedures are the same as those in the synthesis of Ag nanocubes with 204 nm. The reaction proceeded for 2.5 hours, and red suspension was formed finally. In the synthesis of Ag dodecahedra, with the ammonium hydroxide solution, the pH of CPC solution was adjusted from 8.0 to 10.0 before $AgNO_3$ aliquot was added, and the other procedures are the same as those in the synthesis of Ag nanocubes with 204 nm. The green suspension was formed instantly after 150 μL aliquot of Asa solution (100 mM) was added. The reaction was completed within 40 min. The products of Ag nanostructures were collected and washed with warm water twice by centrifugations (8000 rpm, 5 min) for further characterizations.

The ink of Ag nanowires (washed once) was dropped on the glass substrate and dried with the nitrogen flux for the characterization of transparent electrode.

RESULTS AND DISCUSSION

Growth of Ag nanocubes with single-crystalline nanostructures. AgCl nanoparticles were formed by mixing $AgNO_3$ and CPC capping agents solutions at 45 °C. CPC, with the long hydrophobic alkyl chain and hydrophilic ammonium group, not only protects the nanoparticles from aggregation but also controls the growth direction of the noble metal nanostructures in aqueous solution. As shown in the X-ray diffraction (XRD) pattern in Figure 1A, the AgCl precursors exhibit face-centered cubic structure and a strong (200) lattice plane diffraction. Figure S2A shows a Transmission electronic microscopy (TEM) image of the AgCl nanoparticles. The average size of the nanoparticles is 65 ± 13 nm. The high-resolution TEM (HRTEM) image in Figure S2B shows that the measured lattice spacing is 0.206 nm, corresponding to the {220} planes of the face-centered cubic AgCl nanostructures (theoretical spacing, 0.196 nm). The use of solid-state AgCl nanoparticles instead of aqueous $AgNO_3$ solution as the precursor slows down the generation of Ag atoms and facilitates the morphology control of Ag nanostructures. After mixing with Asa (1.2 mM) at 45 °C, the AgCl precursors were reduced into face-centered cubic Ag crystals at the pH value of 8.0, as shown in the XRD pattern in Figure 1A. The intense (200) diffraction peak of the Ag crystals is clearly observed. The diffraction peaks of the AgCl nanoparticles vanish in the XRD pattern, indicating that AgCl precursors are completely reduced to Ag nanocrystals. Figure 1B and 1C show the scanning electronic microscopy (SEM) and TEM images of the as-synthesized Ag nanostructures, respectively.

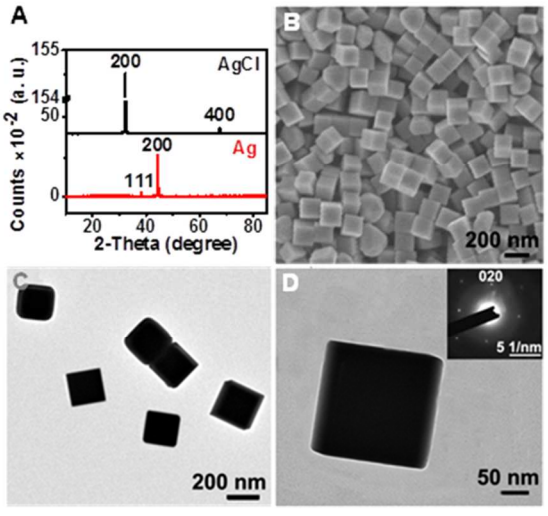

Figure 1. (A) XRD pattern of Ag nanocubes (bottom, JCPDS no. 04-0783), and AgCl nanoparticles formed before Asa was added (top, JCPDS no. 31-1238). (B) SEM and (C) TEM images of Ag nanocubes synthesized at pH 8.0. (D) TEM image of a single Ag cube along the [100] direction and the corresponding SAED pattern (inset).

The majority (> 90%) of as-grown products are with the shape of the nanocubes. The average size is 204 ± 29 nm. Figure 1D shows the TEM image of a single Ag nanocube and the corresponding selected area electron diffraction (SAED) pattern, exhibiting a single crystalline nanostructure along the [100] direction.

The growth process is also reflected in the in-situ monitoring of UV-visible extinction spectra. As shown in Figure S2C, the white AgCl precursor solution has an extinction band around the wavelength of 340 nm. After Asa was added for 4.5 hours, the solution turned into light yellow and an extinction peak at 380 nm appears, and cubic nanostructures (~ 80 nm) are found in the TEM characterizations, as shown in Figure S2D and S2E. In the HRTEM characterization of the single nanocube (Figure S2F), the measured lattice spacing of the nanocube are 0.205 nm and 0.199 nm, which is in agreement with the {100} planes of the face-centered cubic Ag nanostructures (theoretical spacing, 0.204 nm). This indicates that Ag nanocubes enclosed by {100} facets are formed when the reducing reaction proceeds for 4.5 hours. As Ag nanocubes grow, the extinction peak red-shifts and the extinction band of the AgCl precursors vanish gradually. After the reaction for 11 hours, Ag nanocubes were grown up to 204 nm (Figure 1B) and the extinction spectra were unchanged with time any more, indicating that the reducing reaction was completed. During the growth of Ag nanocubes, Ag nanoclusters (~ 4 nm) are found (Figure S2E and S2F), and the measured lattice spacing (0.234 nm) agrees with the {111} planes of the face-centered cubic Ag nanostructures (theoretical spacing, 0.236 nm). It is suggested that Ag nanocubes are grown through the aggregations of small Ag nanoclusters, which are formed during the reductions following the Ostwald ripening mechanism.[32]

Anisotropic growth of Ag nanowires with five-fold multi-crystalline nanostructure. The heterogeneous nucleation is much faster than homogeneous nucleation in solution because the activation energy for the reduction of metal atoms onto a preferred particle is significantly reduced.[20] Trace amounts of Pd nanocubes (33.2 pM) were introduced in the solution at the pH value of 8.0 to accelerate the reducing reaction, resulting in the formation of Ag nanowires. The SEM images in Figure 2A and 2B show that large-scale Ag nanowires are produced (> 95%). The average length and diameter of the Ag nanowires are 3.8 ± 0.8 μm and 28 ± 3.5 nm, respectively. The XRD pattern is shown in Figure S3A, and the intense (111) and (200) diffraction peaks of the face-centered cubic Ag nanowires are observed.[33] Figure 2C shows the TEM images of the Ag nanowires and an enlarged image (inset) of the part marked in the quadrilateral. The corresponded SAED pattern is shown in Figure 2D, and the reflection spots of the [112] and [001] zones of face-centered cubic Ag are clearly observed. It indicates that the Ag nanowire possess a cyclic pentagonal structures and grow along the [110] direction.[34,35] And the five-fold multiply twinned Ag nanowire in Figure 2C is bounded by five {111} end facets and five {100} side facets, laying on the substrate with one

side facet. Figure 2E shows a HRTEM image of the part of the single Ag nanowire. The [111] twin plane is oriented parallel to its longitudinal axis. The aspect-ratio of the as-grown Ag nanowires is 136. We prepared the transparent electrode with the Ag nanowires. The sheet resistance and transmittance are 15 Ω sq-1 and 84.5% (Figure 2F), respectively, comparable to the transparent electrode made with the polyol synthesis Ag nanowires.[16]

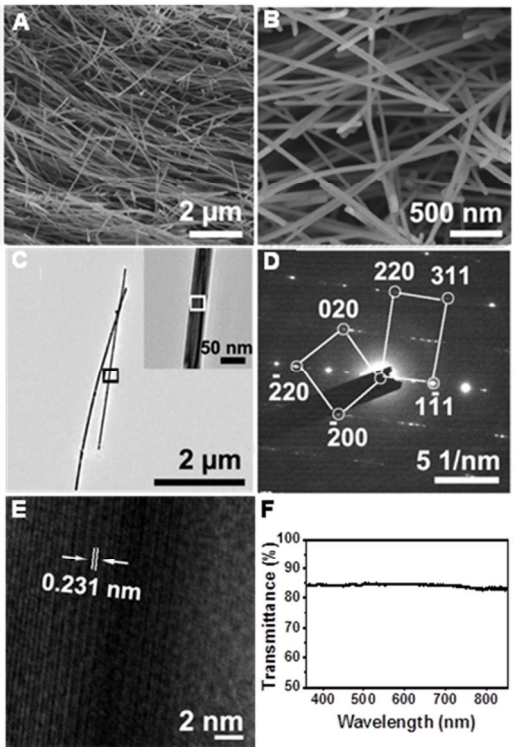

Figure 2. (A, B) SEM images of Ag nanowires produced in the presence of 33.2 pM Pd nanocubes at the pH value of 8.0. (C) TEM image of Ag nanowires. Inset: enlarge image of the part of the single Ag nanowire in the quadrilateral. (D) SAED pattern corresponding to the part of the single Ag nanowire shown in the inset of (C). (E) HRTEM image of the part of the single Ag nanowire in the quadrilateral shown in the inset of (C). (F) Transmittance-wavelength curve of transparent electrode prepared with Ag nanowires.

Compared with the Ag nanocubes formed by homogeneous nucleation, the growth rate of the Ag nanowire is greatly increased. As shown in the in-situ UV-visible extinction spectra in Figure S3B, the reductions of the AgCl precursors into Ag nanowires were completed within 4.5 hours and a milk yellow suspension was formed finally. The TEM image in Figure S3C shows that the Ag nanorods with the length of ~ 200 nm and diameter of ~ 20 nm were formed after the Asa was injected for 1.5 hours. The side surfaces of the Ag nanorods are not even during the growth. The five-fold twinned nanostructure of a single Ag nanorod is exhibited by the HRTEM image and the corresponded fast Fourier transformation (FFT) patterns (Figure S3D).[34,35] And the five-fold twinned nanoparticles are observed in Figure S3C, which may further grow into the long Ag nanowires along the [110] direction. The Pd nanocubes play a role as catalysis to reduce AgCl precursor into Ag atoms, which is critical to the formation of Ag nanowires. It is presumed that the reduction of the AgCl precursors preferentially occurs on the Pd nanocubes.[23] The Ag atoms could separate from the Pd nanocubes after the reduction and form small nanoclusters, which aggregate into new nanostructures (nanowires). Because the CPC molecules can selectively adsorb onto the {100} facets of the Ag nanostructures and stabilize them from disappearing during the anisotropic crystal growth.[36] And the medium reduction rate caused by the trace of Pd nanocubes allows the Ag nanoclusters to aggregate along the [110] direction continuously.[37,38] Therefore, the one-dimensional Ag nanowires are formed eventually.

Thermodynamically-favored Ag triangular bipyramids and cubes with twinned boundaries. By further increasing the concentration of the Pd nanocubes to 1.33 nM, the reduction reaction became faster. The solution became into light green after the Asa was mixed for 30 min. As shown in the in-situ UV-Visible extinction spectra in Figure S4, the reduction was completed within 2.5 hours and the solution became into brick red color. The products were mainly composed of {100}-faceted Ag nanocubes and right-triangular bipyramids (~80%), as shown in the TEM image in Figure 3A. The SAED pattern of a single right-triangular bipyramid along the [100] direction and corresponding TEM image were shown in Figure 3B. A fan-shaped projection was exhibited, which is in agreement with the theoretical model of a right-triangle bipyramid along the same direction (Figure 3C).

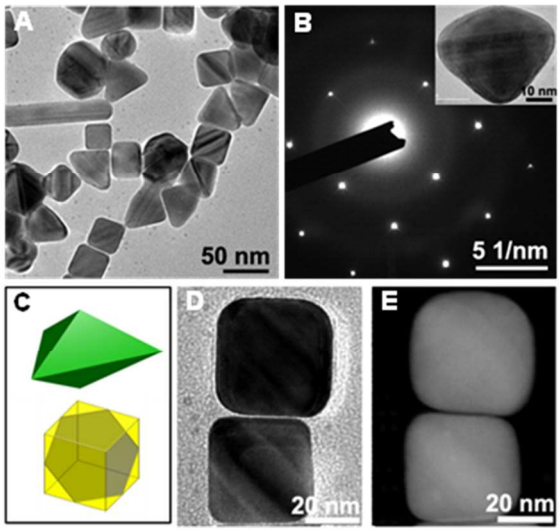

Figure 3. (A) SEM images of Ag nanostructures produced in the presence of 1.33 nM Pd nanocubes at pH 8.0. (B) SAED pattern of a single right-triangular bipyramid with a {100} facet laid on the substrate and corresponded TEM image (inset). (C) Models of the single right-triangular bipyramid (top) and the cube with twinned boundaries (down). (D) Bright field and (E) dark field TEM image of Ag nanocubes with twinned boundaries.

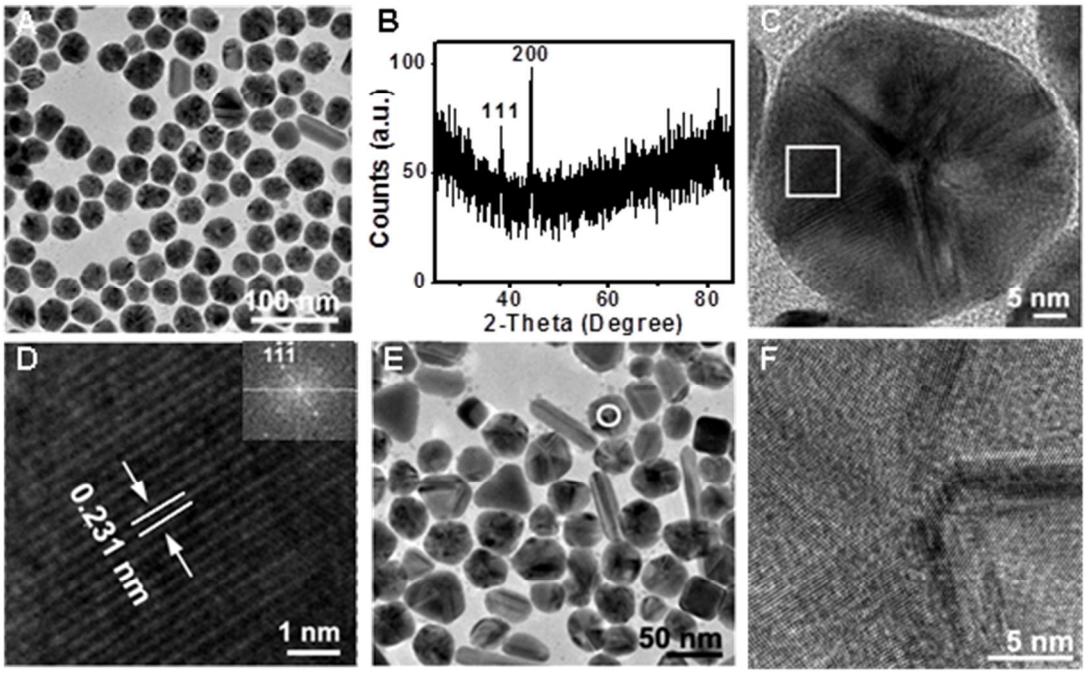

Figure 4. (A) TEM image and (B) XRD pattern of Ag decahedra produced at the pH value of 10.0 with 0.3 mM Asa. (C) TEM image of a single Ag multiply twinned decahedral Ag nanostructures along the five-fold symmetry axis. (D) HRTEM image of the part of a single Ag decahedron in the quadrilateral marked in (C). (E) TEM image of Ag nanostructures produced at the pH value of 10.0 with 1.2 mM Asa. (F) HRTEM image of the central part of a single Ag decahedron in the cycle marked in (E).

The three longitudinal and two transverse vertices are 44.2 ± 3.3 nm and 60.6 ± 4.3 nm, and the ratio fitted with the theoretical value of 1.41.[39] For the {100}-faceted Ag nanocubes with 35.3 ± 3.7 nm, oval twinned boundaries are found to be present diagonally across the cubes, as shown in the bright-field and dark-field TEM images of a single nanocube in Figure 3D and 3E, respectively. The corresponding theoretical model is shown in Figure 3C. The unusual Ag nanocubes with twinned boundaries are used to be obtained in the plasmon-mediated synthesis or the platelet transformation process.[40, 41]

Even in the presence of higher concentration of Pd nanocubes (1.33 nM), there is no Pd signal observed in the nanostructures (Figure 3E). The results are different from the nucleation of gold (Au) atoms on Pd nanocubes, in which Pd-Au core-shell hetero-structures were produced in the same concentration of Pd cubes.[42-44] With much faster reduction rate, the thermodynamically-favored polyhedral Ag nanostructures (right-triangular bipyramids and cubes with twinned boundaries) are formed because of the quick nucleation of metal atoms and depletion of precursor at the initial stage of the reactions, following the Wulff's theorem.[45] The {100} facet becomes the thermodynamically stable surfaces, which are dominant in the products formed through both the homogenous and heterogeneous nucleation at pH 8.0. And the reaction rate determines the anisotropies of the final Ag nanostructures. In the presence of 6.75 nM Pd cubes, Pd elements are observed in the TEM characterizations. As shown in Figure S5 A and B, Moiré patterns formed by the superposition of misfit of the two lattices are observed, which indicates the core-shell nanostructures are present. An FFT pattern of the part of the shell of the nanoparticle fit for the face-centered cubic Ag structures (Figure S5 C). The elemental mapping analysis of a single core-shell nanostructure shows that Pd elements are mainly disperse in the low-right corner and exhibit a cubic shape with the same size of Pd cubes added before the reaction. It confirmed that Pd cubes provide the nucleation sites for Ag atoms. The self-catalysis occurs once Ag atoms nucleate, and Ag nanoclusters are formed quickly and aggregate into new Ag nanostructures (Figure S5 G). And the Pd-Ag core-shell nanostructures should be present in the products shown in Figure 2 and 3.

Kinetically controlled Ag decahedra with five-fold multi-crystalline nanostructure. When the pH of solution was increased to 10.0 by the injection of ammonia, the reduction rate is greatly increased because the reducibility of Asa is stronger at the basic condition. And the kinetics plays the dominant role in the formations of Ag nanocrystals.[44,46,47] Around 95% of the products are {111}-faceted five-fold multiply twinned decahedral Ag nanoparticles, with the average size of 31 ± 3 nm, as shown in Figure 4A. The solution turned into green instantly when 0.3 mM Asa was added, and the reduction was completed within 40 min. Figure 4B shows an XRD pattern of the

products, indicating that the AgCl precursors were completely reduced into Ag nanostructures. The diffraction peaks of (111) and (200) lattice planes of the face-centered cubic Ag crystals are observed. The HRTEM image of the single decahedral Ag nanoparticle along the five-fold symmetry axis is shown in Figure 4C. The decahedron consists of five tetrahedral with twinned by (110) planes. An HRTEM image corresponding to the part of the single Ag decahedra is shown in Figure 4D. The lattice spacing of 0.231 nm on the surface of the decahedron is indexed to the {111} reflection of the face-centered cubic Ag crystals, which is also confirmed by the corresponded FFT pattern in the inset of Figure 4D. When the concentration of Asa is increased to 1.2 mM, larger decahedral Ag nanoparticles were formed, with high ratio of the co-products (~20%), such as nanorods, nanocubes, or nanoprisms, as shown in Figure 4E. The average size of the decahedral Ag nanoparticles is 41 ± 5 nm. Figure 4F shows an HRTEM image of the center of the single decahedra along the five-fold symmetry axis, exhibiting a well five-fold symmetry. The UV-visible extinction of the Ag nanostructures redly shifts around 20 nm because of the larger size of the products (Figure S6). The formation of the higher yield of byproducts (1.2 mM Asa) affects the size of Ag decahedra.

Effects of temperature and capping agents. The reaction is completed in 1.5 h when the temperature is increased to 80 °C at the pH value of 8.0. And the products are mainly composed of Ag nanocubes (~ 84 nm) and nanowires with length of ~ 2 μm and diameter of ~ 67 nm (Figure S7). Compared to the products at 45 °C (Figure 1), the size of Ag cubes are decreased and the yield is low, and there are Ag nanowires formed. This indicated that a slow reduction rate benefit the growth of Ag nanocubes. When cetyltrimethylammonium chloride is used as the capping agents instead of CPC, the products are composed of Ag nanowires, cubes, triangular bipyramids, and five-fold twinned crystalline nanoparticles (Figure S8). When cetyltrimethylammonium bromide is used as the capping agents instead of CPC, the reduction reaction does not occur because the AgBr is stable and difficult to be reduced compared to AgCl (Figure S9). This indicated that the reaction rate and capping agents are critical to the formation of the shape-controlled of Ag nanostructures. Cetylpyridium cations can protect Ag {100} facets through the selective adsorption and benefit the high-yield production of Ag nanocubes. To study the effect of bromide ions on the growth of Ag nanowires, 0.1 mM potassium bromide are introduced into CPC solutions. As shown in Figure S10, Ag triangular bipyramids, cubes, wires are mainly produced. So the effect of trace amount of bromide ions (which may adsorb to the surface of Pd cubes) on the growth of Ag nanowires is negligible.

CONCLUSION

In summary, we develop a new method for synthesizing the morphology-controlled Ag nanostructures in aqueous solution at a low temperature. With the use of AgCl nanoparticles as the precursors, the shape of the Ag nanostructures can be controlled by both thermodynamic and kinetic factors at 45 °C. CPC capping agents can selectively adsorb onto the {100} facets, which become the thermodynamically stable facets. The {100}-faceted Ag nanocubes, nanowires, right-triangular bipyramids, and nanocubes with twinned boundaries are controllably synthesized by tuning kinetic growth factor (reaction rate). The {111}-faceted decahedra are formed at a higher pH value as the kinetically controlled products. This green, cost-effective, large-scale and efficient method provides a distinct roadmap for synthesizing the morphology-controlled Ag nanostructures and shines light on the fundamental understanding on the controllable growth of metal nanocrystals.

ASSOCIATED CONTENT

Supporting Information. TEM and SEM images, UV-visible extinction spectra. This material is available free of charge via the Internet at http://pubs.acs.org.

AUTHOR INFORMATION

Corresponding Author

* E-mail: ychai@ polyu.edu.hk, li.lilly@polyu.edu.hk

Present Addresses

† *Department of Chemistry, Technical University of Denmark, Kemitorvet, Building 207, DK-2800 Kongens Lyngby, Denmark.*

Author Contributions

All authors have given approval to the final version of the manuscript.

ACKNOWLEDGMENT

We acknowledge financial support from the National Natural Science Foundation of China (grant number 61302045) and the Hong Kong Polytechnic University (grant numbers: G-UA51 and H-ZG1N).

REFERENCES

(1) Choi, H. O.; Kim, D. W.; Kim, S. J.; Yang, S. B.; Jung, H.-T. *Adv. Mater.* **2014**, *26*, 4575-4581.
(2) Lee, N.-K.; Yun, S. Y.; Mamidipalli, P.; Salzman, R. M.; Lee, D.; Zhou, T.; Xia, Y. *J. Am. Chem. Soc.* **2014**, *136*, 4363-4368.
(3) Liu, W.; Herrmann, A.-K.; Bigall, N. C.; Rodriguez, P.; Wen, D.; Oezaslan, M.; Schmidt, T. J.; Gaponik, N.; Eychmüller, A. *Acc. Chem. Res.* **2015**, *48*, 154-162.
(4) Lu, G.; De Keersmaecker, H.; Su, L.; Kenens, B.; Rocha, S.; Fron, E.; Chen, C.; Van Dorpe, P.; Mizuno, H.; Hofkens, J.; Hutchison, J. A.; Uji-i, H. *Adv. Mater.* **2014**, *26*, 5124-5128.
(5) Zhu, X.; Radovic-Moreno, A. F.; Wu, J.; Langer, R.; Shi, J. *Nano Today* **2014**, *9*, 478-498.
(6) Zhang, L.; Wang, E. *Nano Today* **2014**, *9*, 132-157.

(7) Lu, F.; Tian, Y.; Liu, M.; Su, D.; Zhang, H.; Govorov, A. O.; Gang, O. *Nano Lett.* **2013**, *13*, 3145-3151.
(8) Nie, S.; Emory, S. R. *Science* **1997**, *275*, 1102-1106.
(9) Zhao, Y.; Xie, Y.; Bao, Z.; Tsang, Y. H.; Xie, L.; Chai, Y. *The J. Phys. Chem. C* **2014**, *118*, 11827-11832.
(10) Zhao, Y.; Xie, Y.; Hui, Y. Y.; Tang, L.; Jie, W.; Jiang, Y.; Xu, L.; Lau, S. P.; Chai, Y. *J. Mater. Chem. C* **2013**, *1*, 4956-4961.
(11) Huang, M. H.; Thoka, S. *Nano Today (2015)*, http://dx.doi.org/10.1016/j.nantod.2015.01.006.
(12) Jing, H.; Zhang, Q.; Large, N.; Yu, C.; Blom, D. A.; Nordlander, P.; Wang, H. *Nano Lett.* **2014**, *14*, 3674-3682.
(13) Mulvihill, M. J.; Ling, X. Y.; Henzie, J.; Yang, P. *J. Am. Chem. Soc.* **2009**, *132*, 268-274.
(14) Zhao, Y.; Liu, X.; Lei, D. Y.; Chai, Y. *Nanoscale* **2014**, *6*, 1311-1317.
(15) Hsu, P.-C.; Kong, D.; Wang, S.; Wang, H.; Welch, A. J.; Wu, H.; Cui, Y. *J. Am. Chem. Soc.* **2014**, *136*, 10593-10596.
(16) Ye, S.; Rathmell, A. R.; Chen, Z.; Stewart, I. E.; Wiley, B. J. *Adv. Mater.* **2014**, *26*, 6670-6687.
(17) Bergin, S. M.; Chen, Y.-H.; Rathmell, A. R.; Charbonneau, P.; Li, Z.-Y.; Wiley, B. J. *Nanoscale* **2012**, *4*, 1996-2004.
(18) Fairfield, J. A.; Ritter, C.; Bellew, A. T.; McCarthy, E. K.; Ferreira, M. S.; Boland, J. J. *ACS Nano* **2014**, *8*, 9542-9549.
(19) Motl, N. E.; Smith, A. F.; DeSantis, C. J.; Skrabalak, S. E. *Chem. Soc. Rev.* **2014**, *43*, 3823-3834.
(20) Tao, A. R.; Habas, S.; Yang, P. *Small* **2008**, *4*, 310-325.
(21) Zhang, L.; Niu, W.; Xu, G. *Nano Today* **2012**, *7*, 586-605.
(22) Skrabalak, S. E.; Xia, Y. *ACS Nano* **2009**, *3*, 10-15.
(23) Sun, Y.; Xia, Y. *Adv. Mater.* **2002**, *14*, 833-837.
(24) Wiley, B. J.; Xiong, Y.; Li, Z.-Y.; Yin, Y.; Xia, Y. *Nano Lett.* **2006**, *6*, 765-768.
(25) Huang, G.-W.; Xiao, H.-M.; Fu, S.-Y. *Nanoscale* **2014**, *6*, 8495-8502.
(26) Lee, J.; Lee, P.; Lee, H.; Lee, D.; Lee, S. S.; Ko, S. H. *Nanoscale* **2012**, *4*, 6408-6414.
(27) Yang, C.; Gu, H.; Lin, W.; Yuen, M. M.; Wong, C. P.; Xiong, M.; Gao, B. *Adv. Mater.* **2011**, *23*, 3052-3056.
(28) Personick, M. L.; Mirkin, C. A. *J. Am. Chem. Soc.* **2013**, *135*, 18238-18247.
(29) Chang, I. C.; Chen, P.-C.; Tsai, M.-C.; Chen, T.-T.; Yang, M.-H.; Chiu, H.-T.; Lee, C.-Y. *CrystEngComm* **2013**, *15*, 2363-2366.
(30) Yu, T.; Kim, D. Y.; Zhang, H.; Xia, Y. *Angew. Chem. Int. Ed.* **2011**, *50*, 2773-2777.
(31) Niu, W.; Li, Z.-Y.; Shi, L.; Liu, X.; Li, H.; Han, S.; Chen, J.; Xu, G. *Cryst. Growth Des.* **2008**, *8*, 4440-4444.
(32) Lu, C.-L.; Prasad, K. S.; Wu, H.-L.; Ho, J.-a. A.; Huang, M. H. *J. Am. Chem. Soc.* **2010**, *132*, 14546-14553.
(33) Sun, X. M.; Li, Y. D. *Adv. Mater.* **2005**, *17*, 2626-2630.
(34) Lu, N.; Chen, W.; Fang, G.; Chen, B.; Yang, K.; Yang, Y.; Wang, Z.; Huang, S.; Li, Y. *Chem. Mater.* **2014**, *26*, 2453-2459.
(35) Yang, H.-J.; He, S.-Y.; Tuan, H.-Y. *Langmuir* **2013**, *30*, 602-610.
(36) Niu, W.; Zheng, S.; Wang, D.; Liu, X.; Li, H.; Han, S.; Chen, J.; Tang, Z.; Xu, G. *J. Am. Chem. Soc.* **2008**, *131*, 697-703.
(37) Kou, X.; Zhang, S.; Yang, Z.; Tsung, C.-K.; Stucky, G. D.; Sun, L.; Wang, J.; Yan, C. *J. Am. Chem. Soc.* **2007**, *129*, 6402-6404.
(38) Xiong, Y.; Xia, Y. *Adv. Mater.* **2007**, *19*, 3385-3391.
(39) Zhang, J.; Li, S.; Wu, J.; Schatz, G. C.; Mirkin, C. A. *Angew. Chem. Int. Ed.* **2009**, *48*, 7787-7791.
(40) Personick, M. L.; Langille, M. R.; Zhang, J.; Wu, J.; Li, S.; Mirkin, C. A. *Small* **2013**, *9*, 1947-1953.
(41) McEachran, M.; Kitaev, V. *Chem. Commun.* **2008**, *44*, 5737-5739.
(42) Zhang, L.; Niu, W.; Li, Z.; Xu, G. *Chem. Commun.* **2011**, *47*, 10353-10355.
(43) Ding, Y.; Fan, F.; Tian, Z.; Wang, Z. L. *J. Am. Chem. Soc.* **2010**, *132*, 12480-12486.
(44) Zhang, L.; Niu, W.; Gao, W.; Qi, L.; Lai, J.; Zhao, J.; Xu, G. *ACS Nano* **2014**, *8*, 5953-5958.
(45) LaMer, V. K.; Dinegar, R. H. *J. Am. Chem. Soc.* **1950**, *72*, 4847-4854.
(46) Huang, M. H.; Lin, P.-H. *Adv. Funct. Mater.* **2012**, *22*, 14-24.
(47) Niu, W.; Xu, G. *Nano Today* **2011**, *6*, 265-285.

The table of contents

Large-scale morphology-tailored Ag nanostructures capped by cetylpyridinium chloride were produced by reducing AgCl precursors with ascorbic acid at 45℃ in water. Nanocubes, nanowires, triangular bi-pyramids/cubes with twinned boundaries, and decahedra were obtained at different reduction rates (pH, catalysis of Pd cubes). This method is high-efficiency, low-cost, and environmental friendly, opening up a new stage for synthesizing Ag nanostructures.

Ling Zhang, Yuda Zhao, Ziyuan Lin, Fangyuan Gu, Shu Ping Lau, Li Li, and Yang Chai**

Kinetically Controlled Synthesis of Large-Scale Morphology-Tailored Silver Nanostructures at Low Temperature